sodes, and that oxidative stress plays a crucial role not only in the brain lesions of stroke-like episodes [11, 12] but also systemically in these patients. In other words, a history of stroke-like episodes indicates that patients who have these episodes are exposed to underlying oxidative stress.

In the 'non-stroke type' patients, the mean d-ROMs level (oxidative stress) was not significantly different compared with that of the controls (fig. 2a). Meanwhile, the BAP levels (antioxidant activity) were significantly decreased (fig. 2b). Only 1 of 4 patients was treated with antioxidants, and antioxidant therapy may not affect antioxidant activity in 'non-stroke type' patients. These findings may reflect that antioxidants are consumed in order to prevent increase of oxidative stress in these patients. In addition, the difference of profiles in redox states between 'stroke type' and 'non-stroke type' suggested phenotypic diversity in patients carrying A3243G.

In the present study, we presented redox states in the serum of patients carrying A3243G using the d-ROMs and BAP tests. Rapid evaluation of redox states in serum has been difficult to date. To assay oxidative stress in serum, the spin trap method using electron spin resonance (ESR) has been the most reliable method [24]. However, performing ESR is cumbersome, thus it is difficult to apply this method in clinical practice. The d-ROMs test can evaluate oxidative stress in serum by measuring oxides due to hydroperoxides, and this test has been validated by ESR [25]. Likewise, each endogenous antioxidant can be measured, but there has been no method estimating the whole activity of endogenous antioxidants in serum to date. The BAP test provides a reliable indicator of the antioxidant activity in serum by measuring the ability to reduce ferric to ferrous ions [15]. Moreover, the d-ROMs and BAP tests only need a small amount of blood, and require only 15 min for measurement. Therefore, these methods are prompt and reliable, and suitable for evaluating redox states in patients.

Previous studies using postmortem organs or positron emission tomography imaging have demonstrated regional enhancement of oxidative stress in the brain lesions of stroke-like episodes and the heart lesions of cardiomyopathy in patients carrying A3243G [11–13]. Although enhanced oxidative stress due to A3243G has been proven in these lesions, systemic oxidative stress in patients carrying A3243G has not been evaluated to date. The present study demonstrated a systemic and underlying imbalance of redox states in these patients.

The present study has some limitations. (1) The 'non-stroke type' group included only 4 patients. (2) The mean age of 'non-stroke type' patients was likely older than that of 'stroke type' patients. (3) The 'stroke type' group included only 2 of 10 patients with cardiomyopathy or diabetes, which might affect the systemic redox states. (4) All of the 10 'stroke type' patients received antioxidant therapy, but only 1 of the 4 'non-stroke type' patients received antioxidant therapy. (5) This study did not show any significant difference in either value of oxidative stress or antioxidant activity between the 'stroke type' and 'non-stroke type' groups. (6) The possibility that the 'non-stroke type' patients in this study will also subsequently develop stroke-like episodes cannot be ruled out. Further studies are necessary to confirm our preliminary results.

Taken together, the d-ROMs and BAP tests clearly demonstrated an abnormality of redox states in patients carrying A3243G. In particular, enhanced oxidative stress in patients with a history of stroke-like episodes may reflect severe mitochondrial dysfunction, which would contribute to the emergence of stroke-like episodes. In addition, in patients without stroke-like episodes, consumption of antioxidant activity may indicate latent oxidative stress. These findings suggested that patients carrying A3243G are always exposed to underlying oxidative stress, and further antioxidant therapy would be beneficial to prevent an intensification of the symptoms.

Acknowledgement

This study was funded in part by the Scientific Research on Innovative Areas (2020021) and Young Scientists (B) (23790985) from the Japan Society for the Promotion of Science.

Disclosure Statement

The authors report no conflicts of interest.

References

1 Goto Y, Nonaka I, Horai S: A mutation in the tRNA(Leu)(UUR) gene associated with the MELAS subgroup of mitochondrial encephalomyopathies. Nature 1990;348:651–653.
2 Pavlakis SG, Phillips PC, DiMauro S, De Vivo DC, Rowland LP: Mitochondrial myopathy, encephalopathy, lactic acidosis, and strokelike episodes: a distinctive clinical syndrome. Ann Neurol 1984;16:481–488.
3 Vilarinho L, Santorelli FM, Rosas MJ, Tavares C, Melo-Pires M, DiMauro S: The mitochondrial A3243G mutation presenting as severe cardiomyopathy. J Med Genet 1997;34:607–609.

4 Silvestri G, Bertini E, Servidei S, Rana M, Zachara E, Ricci E, Tonali P: Maternally inherited cardiomyopathy: a new phenotype associated with the A to G AT nt.3243 of mitochondrial DNA (MELAS mutation). Muscle Nerve 1997;20:221–225.
5 van den Ouweland JM, Lemkes HH, Ruitenbeek W, Sandkuijl LA, de Vijlder MF, Struyvenberg PA, van de Kamp JJ, Maassen JA: Mutation in mitochondrial tRNA(Leu) (UUR) gene in a large pedigree with maternally transmitted type II diabetes mellitus and deafness. Nat Genet 1992;1:368–371.
6 Reardon W, Ross RJ, Sweeney MG, Luxon LM, Pembrey ME, Harding AE, Trembath RC: Diabetes mellitus associated with a pathogenic point mutation in mitochondrial DNA. Lancet 1992;340:1376–1379.
7 Zhang J, Yoneda M, Naruse K, Borgeld HJ, Gong JS, Obata S, Tanaka M, Yagi K: Peroxide production and apoptosis in cultured cells carrying mtDNA mutation causing encephalomyopathy. Biochem Mol Biol Int 1998;46:71–79.
8 Rusanen H, Majamaa K, Hassinen IE: Increased activities of antioxidant enzymes and decreased ATP concentration in cultured myoblasts with the 3243A–>G mutation in mitochondrial DNA. Biochim Biophys Acta 2000;1500:10–16.
9 Pang CY, Lee HC, Wei YH: Enhanced oxidative damage in human cells harboring A3243G mutation of mitochondrial DNA: implication of oxidative stress in the pathogenesis of mitochondrial diabetes. Diabetes Res Clin Pract 2001;54:S45–S56.
10 Indo HP, Davidson M, Yen HC, Suenaga S, Tomita K, Nishii T, Higuchi M, Koga Y, Ozawa T, Majima HJ: Evidence of ROS generation by mitochondria in cells with impaired electron transport chain and mitochondrial DNA damage. Mitochondrion 2007;7:106–118.
11 Katayama Y, Maeda K, Iizuka T, Hayashi M, Hashizume Y, Sanada M, Kawai H, Kashiwagi A: Accumulation of oxidative stress around the stroke-like lesions of MELAS patients. Mitochondrion 2009;9:306–313.
12 Ikawa M, Okazawa H, Arakawa K, Kudo T, Kimura H, Fujibayashi Y, Kuriyama M, Yoneda M: PET imaging of redox and energy states in stroke-like episodes of MELAS. Mitochondrion 2009;9:144–148.
13 Ishikawa K, Kimura S, Kobayashi A, Sato T, Matsumoto H, Ujiie Y, Nakazato K, Mitsugi M, Maruyama Y: Increased reactive oxygen species and anti-oxidative response in mitochondrial cardiomyopathy. Circ J 2005;69:617–620.
14 Cesarone MR, Belcaro G, Carratelli M, Cornelli U, De Sanctis MT, Incandela L, Barsotti A, Terranova R, Nicolaides A: A simple test to monitor oxidative stress. Int Angiol 1999;18:127–130.
15 Benzie IF, Strain JJ: The ferric reducing ability of plasma (FRAP) as a measure of 'antioxidant power': the FRAP assay. Anal Biochem 1996;239:70–76.
16 Gerardi G, Usberti M, Martini G, Albertini A, Sugherini L, Pompella A, Di LD: Plasma total antioxidant capacity in hemodialyzed patients and its relationships to other biomarkers of oxidative stress and lipid peroxidation. Clin Chem Lab Med 2002;40:104–110.
17 Dohi K, Satoh K, Ohtaki H, Shioda S, Miyake Y, Shindo M, Aruga T: Elevated plasma levels of bilirubin in patients with neurotrauma reflect its pathophysiological role in free radical scavenging. In Vivo 2005;19:855–860.
18 Yamanaka G, Kawashima H, Suganami Y, Watanabe C, Watanabe Y, Miyajima T, Takekuma K, Oguchi S, Hoshika A: Diagnostic and predictive value of CSF d-ROM level in influenza virus-associated encephalopathy. J Neurol Sci 2006;243:71–75.
19 Braekke K, Bechensteen AG, Halvorsen BL, Blomhoff R, Haaland K, Staff AC: Oxidative stress markers and antioxidant status after oral iron supplementation to very low birth weight infants. J Pediatr 2007;151:23–28.
20 Nakayama K, Terawaki H, Nakayama M, Iwabuchi M, Sato T, Ito S: Reduction of serum antioxidative capacity during hemodialysis. Clin Exp Nephrol 2007;11:218–224.
21 Kakita H, Hussein MH, Yamada Y, Henmi H, Kato S, Kobayashi S, Ito T, Kato I, Fukuda S, Suzuki S, Togari H: High postnatal oxidative stress in neonatal cystic periventricular leukomalacia. Brain Dev 2009;31:641–648.
22 Nishikawa T, Okamoto Y, Kodama Y, Tanabe T, Shinkoda Y, Kawano Y: Serum derivative of reactive oxygen metabolites (d-ROMs) in pediatric hemato-oncological patients with neutropenic fever. Pediatr Blood Cancer 2010;55:91–94.
23 Esposito LA, Melov S, Panov A, Cottrell BA, Wallace DC: Mitochondrial disease in mouse results in increased oxidative stress. Proc Natl Acad Sci USA 1999;96:4820–4825.
24 Buettner GR: Spin trapping: ESR parameters of spin adducts. Free Radic Biol Med 1987;3:259–303.
25 Alberti A, Bolognini L, Macciantelli D, Carratelli M: The radical cation of N,N-diethyl-para-phenylendiamine: a possible indicator of oxidative stress in biological samples. Res Chem Intermed 2000;26:253–267.

JOURNAL OF MEDICAL CASE REPORTS

CASE REPORT Open Access

A two-day-old hyperthyroid neonate with thyroid hormone resistance born to a mother with well-controlled Graves' disease: a case report

Shuichi Yatsuga[1*], Yuji Hiromatsu[2], Shigekazu Sasaki[3], Hirotoshi Nakamura[3], Koju Katayama[1], Junko Nishioka[1] and Yasutoshi Koga[1]

Abstract

Introduction: Resistance to thyroid hormone is a syndrome caused by thyroid hormone receptor β mutations, which are usually inherited in an autosomal-dominant pattern.

Case presentation: Our patient, a Japanese neonate boy, showed hyperthyroid symptoms at age two days. Although our patient was diagnosed as having resistance to thyroid hormone, his hyperthyroid symptoms continued for two weeks. Therefore, our patient was treated with methimazole and iodine for two weeks from birth, showing no side effects and no symptoms upon treatment. At age 70 days, an R243W mutation in thyroid hormone receptor β was detected in our patient; while absent in his mother, the mutation was present in his father, who never showed any symptoms.

Conclusions: To the best of our knowledge this is the first case report of a resistance to thyroid hormone in a neonate presenting with hyperthyroid symptoms born to a mother with Graves' disease and treated with methimazole and iodine. These results suggest that methimazole and iodine may be a good short-term option for treatment.

Keywords: Hyperthyroid symptoms, Maternal Graves' disease, Symptomatic neonate with resistance to thyroid hormone, Treatment for resistance to thyroid hormone

Introduction

Resistance to thyroid hormone (RTH) is an autosomal dominant (AD) syndrome in which an individual's response to thyroid hormone (TH) is decreased due to mutations in the TH receptor β gene (*TRβ*) [1,2]. Patients with RTH have increased serum TH levels and increased or normal thyroid-stimulating hormone (TSH) levels. The clinical characteristics of RTH vary strikingly, as even the characteristics of various tissues within the same individual or family members who carry identical mutations differ notably [3]. While most patients are asymptomatic, some are symptomatic and show main clinical features such as goiter, hyperactivity, and tachycardia [1]. However, although RTH has been well investigated recently, the response of patients with RTH to treatment remains unclear.

A neonate born to a mother with Graves' disease (GD) has an increased risk of developing neonatal GD, a rare condition that affects 1% to 5% of babies born to mothers who have hyperthyroidism during pregnancy. Most babies are asymptomatic because the mother normally receives treatment for her GD. In contrast, patients with RTH do not usually receive treatment because they show no symptoms. Indeed, even when they do show symptoms, the results of treatment have been discouraging. Kim *et al.* treated one symptomatic patient with RTH with methimazole (MMI) and T_4 treatment but had to cease treatment because a large goiter developed [4], improving upon treatment withdrawal.

Here, we describe a symptomatic neonate with an R243W *TRβ* mutation inherited from his non-symptomatic father. Our patient, who was born to a

* Correspondence: yatsuga_shyuuichi@med.kurume-u.ac.jp
[1]Department of Pediatrics and Child Health, Kurume University School of Medicine, 67 Asahi-Machi, Kurume, Fukuoka 830-0011, Japan
Full list of author information is available at the end of the article

mother with well-controlled GD, continued to show hyperthyroid symptoms for two weeks, at which point we administered MMI and iodine for another two weeks and monitored our patient's symptoms and thyroid function tests.

Case presentation

Our patient's parents were non-consanguineous and of Japanese origin, with an unremarkable family history except for the mother, who had thyroid symptoms. The mother had an onset of GD at 23 years of age and was subsequently treated for hyperthyroidism with 30mg/day MMI and 50mg/day iodine potassium. After two weeks of treatment, our patient's mother experienced side effects from the MMI, and the regimen was therefore changed to 300mg/day of propylthiouracil (PTU). The PTU dose was then reduced gradually as thyroid hormone levels improved. The mother became pregnant seven months after the GD diagnosis and was treated with 50mg PTU every two days. Thyroid hormones and antibodies related to GD in the mother were within normal ranges throughout the pregnancy (Table 1).

Our patient was born at 38 weeks into the pregnancy following a non-problematic gestation period. His birth weight was 2910g. Our patient exhibited visible hyperthyroid symptoms two days after birth, including tachycardia, frequent bowel movements, and hyper-irritability. A complete blood cell count and blood chemistry examination revealed normal levels with the exception of increased thyroid hormone levels (Table 1). Antibodies associated with thyroid disease were within normal ranges (Table 1). Electrocardiography primarily showed a regular sinus rhythm, and our patient's sleeping heart rate was slightly elevated at 150 to 160 beats per minute compared with the normal range of 120 to 140 beats per minute. Ultrasonography revealed the thyroid to be normal in size with no nodules. A TSH-secreting adenoma (TSHoma) was ruled out through magnetic resonance imaging (MRI) scans of the pituitary gland, and our patient's human chorionic gonadotropin β (hCG-β) levels were found to be normal at admission. Our patient was suspected of having RTH rather than neonatal GD due to unsuppressed TSH and high free T_4 (FT_4) and T_3 (FT_3) levels.

At 14 days old, our patient still continued to show hyperthyroid symptoms and was therefore treated with 0.65mg/kg/day MMI and 12.6mg/day iodine. Our patient responded to the therapy clinically. His irritability diminished, and his sleeping heart rate reduced to 130 to 150 beats per minute. Expectedly, his TSH level increased, and his FT_4 and FT_3 levels decreased (Figure 1). During this course, our patient presented no elevation of antibodies related to GD, and an abnormal thyroid hormone profile continued without goiter. MMI and iodine were discontinued at age 28 days, as our patient's symptoms, particularly hyper-irritability and frequent bowel movements, were improved. In the two-week treatment period, our patient showed neither severe nor worsening symptoms. Our patient was hospitalized for a total of 33 days before being discharged, at which point our patient was confirmed to be euthyroid; follow-up was conducted every three months using thyroid function tests. Today, our patient is three years old and remains clinically euthyroid without the use of therapeutic drugs after discharge. Our patient has also reached developmental milestones appropriate for his age.

Our patient's bone development was also normal, and his electrocardiography, Holter electrocardiography, and echocardiogram findings were all within normal limits, with no severe cardiac complications observed. Our patient's father had never experienced symptoms of hypothyroid or hyperthyroidism, although inappropriate thyroid hormone levels were seen in laboratory tests (Table 1).

Table 1 Thyroid hormone profile of our patient and his mother and father

Profile and normal range	Onset	P0	P5	P8	Delivery	Patient's father	Patient
TSH (μIU/mL) (0.4 to 4.0)	0	0	0.61	0.27	0.04	0.59	5.38 (1.0 to 38.9)
FT_4 (ng/dL) (0.8 to 1.9)	5.64	1.53	0.83	0.9	1.16	2.87	4.76 (2.0 to 4.9)
FT_3 (pg/mL) (2.2 to 4.1)	22.38	2.65	1.93	2.27	NA	4.88	6.7 (2.0 to 6.1)
TgAb (IU/mL) (<28)	0.3	0.3	0.3	0.3	NA	0.3	<0.1 (<28)
TPOAb (IU/mL) (<16)	9.1	0.7	0.3	0.3	NA	<0.3	<0.1 (<16)
TRAb (IU/L) (<1)	15	4	1.2	1	NA	<0.1	<0.1 (<1)
TSAb (%) (<180)	188	239	135	132	NA	130	173 (<180)
Tg (ng/mL) (<32.7)	540	130	68	NA	NA	NA	NA

Thyroid hormone profile of the mother (onset of GD to child delivery), the father, and our patient at two days after birth. P0 is zero months' pregnant, P5, five months' pregnant, P8, eight months' pregnant. Values at onset and P0 indicate typical Graves' disease (GD). GD was well controlled during pregnancy by propylthiouracil. Reference values for adults are used for the mother and the father; reference values for neonates are used for our patient. In the father and our patient, all values for thyroid antibodies were negative, indicating resistance to thyroid hormone. Thyroid-stimulating antibody (TSAb) was measured using radioimmunoassay (RIA), while all other values were measured using electrochemiluminescence immunoassay (ECLIA).
FT_3/T_4, free T_3/T_4; Tg, thyroglobulin; TgAb, thyroglobulin antibody; TPOAb, thyroid peroxidase antibody; TRAb, TSH receptor antibody; NA, not available.

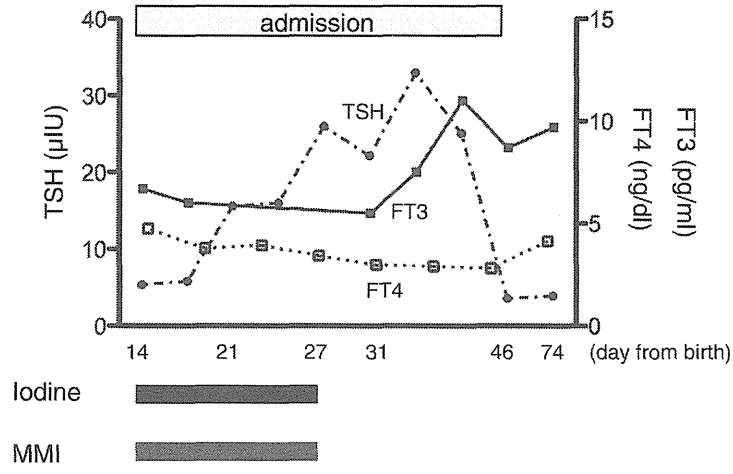

Figure 1 Thyroid hormone and treatment course of our patient during and after admission. After increasing methimazole (MMI) and iodine dosage, thyroid-stimulating hormone (TSH) levels were increased while those of free T_4 (FT_4) and FT_3 were decreased. When MMI and iodine were not administered, TSH fell back to normal levels, while FT_4 and FT_3 increased. Administered iodine and MMI doses are shown in black and gray squares, respectively.

Blood samples were obtained from our patient and both his parents, and genomic deoxyribonucleic acid (DNA) was isolated from leukocytes using standard protocols. Sequencing the patient's *TRβ* gene revealed a missense mutation that causes an R243W substitution within the receptor's T_3-binding domain. While the mother's *TRβ* gene did not contain this mutation, the father's did.

Discussion

This case report describes a baby boy with a *TRβ* R243W mutation born to a mother with no RTH mutation and with no family history of RTH. Our patient's asymptomatic father carried the same mutation as our patient.

The R243W point mutation, first detected by Pohlenz *et al.* [5], has a mechanism of action differing from that of other *TRβ* mutations, as the R243W receptor has normal T_3-binding affinity but transactivates poorly upon binding T_3, thereby conferring a dominant-negative effect [6,7]. The resulting phenotype is usually euthyroid with occasional hypothyroidism being observed. Regardless, clinical features of both hypothyroidism and hyperthyroidism are expected due to variable resistance in the different tissues of an individual. In the present case, a small amount of PTU from the mother transmitted to the fetus may have induced hyperthyroidism just after birth. Since such quantities of PTU may slightly suppress thyroid hormones in the fetus, a sudden release of thyroid hormones after birth may have occurred, causing our patient to be initially diagnosed as having hyperthyroidism.

The clinical phenotype for R243W also differs among families and individuals. In fact, the same mutation can cause either generalized RTH or pituitary RTH in different individuals within the same family. For example, a boy who had slight attention-deficit hyperactivity disorder and the R243W mutation was born to a mother who remained clinically euthyroid with the same mutation [8]. Additionally, only a weak correlation has been observed between a given mutation and the development of RTH [1,3,9]. In rare cases, RTH coexists with GD [10,11]. Considering the mother's condition in the present case, it would be normal for our patient to be suspected of having neonatal GD. However, since our patient showed no suppressed TSH levels and had high FT_4 and FT_3 levels with no antibodies related to GD, our patient was diagnosed as having RTH.

Patients with RTH are not usually treated because many patients do not have significant symptoms. Kim et al. administered MMI plus T_4 treatment for a symptomatic 11-month-old patient who had hyperthyroidism secondary to RTH [4]. However, a large goiter developed without clinical improvements, and after withdrawing treatment, the goiter then improved. In the present case, we treated our patient with MMI and iodine for two weeks, after which our patient showed improved hyperthyroid symptoms and no goiter. In the report by Kim *et al.*, the patient had severe symptoms, including a failure to thrive, verbal delays and tachycardia. Our patient had symptoms of tachycardia, diarrhea, and hyperirritability but showed no failure to thrive or developmental delay, an aspect we attribute to our treatment program.

The differential diagnoses in the present case were neonatal GD and TSHoma. TSHoma can be discovered relatively easily using magnetic resonance imaging

(MRI); however, when a pregnant mother has GD, a neonate with hyperthyroid symptoms is typically expected to have neonatal GD, which can often lead to a misdiagnosis of RTH [10]. Consulting previous papers, which showed how to diagnose RTH with thyroid diseases [12,13], would have avoided such a misdiagnosis.

Conclusions

We describe the case of a neonate presenting with hyperthyroid symptoms. In hyperthyroid neonates born to mothers with GD, it is important to examine the thyroid hormone levels of both parents. Had serum TSH receptor antibody (TRAb) or thyroid-stimulating antibody (TSAb) been elevated in both our patient and his mother, diagnosis of RTH would have been further delayed. To the best of our knowledge this is the first report of a symptomatic neonate with RTH born to a mother with GD and treated by MMI and iodine in the neonatal period without side effects. MMI and iodine, therefore, may make for optimal short-term treatment in hyperthyroid RTH neonates.

Consent

Written informed consent was obtained from the patient's next-of-kin for publication of this case report and any accompanying images. A copy of the written consent is available for review from the Editor-in-Chief of this journal.

Competing interests

The authors report no financial competing interests.

Authors' contributions

SY, YH, KK, JN, and YK examined our patient and discussed the diagnosis and treatment. SS and HN carried out the molecular genetic study, and SY drafted the manuscript. All authors read and approved the final manuscript.

Acknowledgements

The genetic diagnostics completed in this study were supported by the Department of Internal Medicine, Hamamatsu University School of Medicine, Shizuoka, Japan.

Author details

[1]Department of Pediatrics and Child Health, Kurume University School of Medicine, 67 Asahi-Machi, Kurume, Fukuoka 830-0011, Japan. [2]Department of Medicine, Division of Endocrinology and Metabolism, Kurume University School of Medicine, 67 Asahi-Machi, Kurume, Fukuoka 830-0011, Japan. [3]Department of Internal Medicine, Hamamatsu University School of Medicine, 1-20-1 Handayama, Hamamatsu, Shizuoka 431-3192, Japan.

Received: 8 February 2012 Accepted: 8 June 2012
Published: 20 August 2012

References

1. Refetoff S, Weiss RE, Usala SJ: **The syndromes of resistance to thyroid hormone.** *Endocr Rev* 1993, 14:348–399.
2. Weiss RE, Refetoff S: **Treatment of resistance to thyroid hormone-primum non nocere.** *J Clin Endocrinol Metab* 1999, 84:401–404.
3. Beck-Peccoz P, Chatterjee VK: **The variable clinical phenotype in thyroid hormone resistance syndrome.** *Thyroid* 1994, 4:225–232.
4. Kim TJ, Travers S: **Case report: thyroid hormone resistance and its therapeutic challenges.** *Curr Opin Pediatr* 2008, 20:490–493.
5. Pohlenz J, Schönberger W, Wemme H, Winterpacht A, Wirth S, Zabel B: **New point mutation (R243W) in the hormone binding domain of the c-erbA β1 gene in a family with generalized resistance to thyroid hormone.** *Hum Mutat* 1996, 7:79–81.
6. Collingwood TN, Wagner R, Matthews CH, Clifton-Bligh RJ, Gurnel M, Rajanayama O, Agostini M, Fletterick RJ, Beck-Peccoze P, Reinhardt W, Binder G, Ranke MB, Hermus A, Hesch RD, Lazarus J, Newrick P, Parfitt V, Raggatt P, de Zegher F, Chatterjee VK: **A role for helix 3 of the TRβ ligand-binding domain in coactivator recruitment identified by characterization of a third cluster of mutations in resistance to thyroid hormone.** *EMBO J* 1998, 17:4760–4770.
7. Yagi H, Pohlenz J, Hayashi Y, Sakurai A, Refetof S: **Resistance to thyroid hormone caused by two mutant thyroid hormone recepterβ, R243Q and R243W, with marked impairment of function that cannot be explained by altered *in vitro* 3,5,3′-triiodothyroinine binding affinity.** *J Clin Endocrinol Metab* 1997, 82:1608–1614.
8. Massaad D, Poppe K, Lissens W, Velkeniers B: **A case of thyroid hormone resistance: prospective follow-up during pregnancy and obstetric outcome.** *Eur J Intern Med* 2007, 18:253–254.
9. Brucker-Davis F, Skarulis MC, Grace MB, Benichou J, Hauser P, Weintraub Wiggs E: **Genetic and clinical features of 42 kindreds with resistance to thyroid hormone. The National Institutes of Health Prospective Study.** *Ann Intern Med* 1995, 123:572–583.
10. Sivakumar T, Chaidarun S: **Resistance to thyroid hormone in a patient with coexisting Graves' disease.** *Thyroid* 2010, 20:213–216.
11. Sato H: **Clinical features of primary hyperthyroidism caused by Graves' disease admixed with resistance to thyroid hormone (P453T).** *Endocr J* 2010, 57:687–692.
12. Lafranchi SH, Snyder DB, Sesser DE, Skeels MR, Singh N, Brent GA, Nelson JC: **Follow-up of newborns with elevated screening T4 concentrations.** *J Pediatr* 2003, 143:296–301.
13. Fisher DA: **Neonatal hyperthyroid screening.** *J Pediatr* 2003, 143:285–287.

doi:10.1186/1752-1947-6-246
Cite this article as: Yatsuga *et al.*: A two-day-old hyperthyroid neonate with thyroid hormone resistance born to a mother with well-controlled Graves' disease: a case report. *Journal of Medical Case Reports* 2012 6:246.

In Vitro Cell.Dev.Biol.—Animal (2012) 48:313–325
DOI 10.1007/s11626-012-9508-x

Strategies to detect interdigital cell death in the frog, *Xenopus laevis*: T_3 accerelation, BMP application, and mesenchymal cell cultivation

Keiko Shimizu-Nishikawa · Shin-ichiro Nishimatsu · Akio Nishikawa

Received: 30 November 2011 / Accepted: 3 April 2012 / Published online: 12 May 2012 / Editor: T. Okamoto

Abstract Fates of digits in amniotes, i.e., free or webbed digits, are determined by the size of programmed interdigital cell death (ICD) area. However, no (or very few) cell death has thus far been observed in developing limb buds of non-amniotic terrestrial vertebrates including other anuran or urodela amphibians. We speculate that the undetectable situation of amphibian ICD is the result of their less frequency due to slow developmental speed characteristic to most amphibian species. Here, we present three strategies for detecting difficult-to-find ICD in the frog, *Xenopus laevis*. (1) Addition of triiodo-L-thyronine (T_3) accelerated two to three times the limb development and increased two to four times the appearance frequency of vital dye-stainable cells in limb buds of the accelerated tadpoles (stage 54 to 55). (2) Application of human bone morphogenetic protein-4 to the autopods of tadpoles at stage 53 to 54 enhanced digital cartilage formation and induced vital dye-stainable cells around the enhanced digital cartilages within 2 d. (3) In cell culture, T_3 increased the chondrogenic and cell death activities of limb mesenchymal cells. The augmentation of both activities by T_3 was stronger in the forelimb cells than in the hindlimb cells. This situation is well coincided with the limb fates of non-webbed forelimbs and webbed hindlimbs in *X. laevis* adulthood. Collectively, all three approaches showed that it become possible to detect *X. laevis* ICD with appropriate strategies.

K. Shimizu-Nishikawa · A. Nishikawa (✉)
Department of Biological Science,
Faculty of Life and Environmental Science, Shimane University,
1060 Nishikawatsu,
Matsue, Shimane 690-8504, Japan
e-mail: akio@life.shimane-u.ac.jp

S.-i. Nishimatsu
Department of Molecular Biology, Kawasaki Medical School,
577 Matsushima,
Kurashiki, Okayama 701-0192, Japan

Keywords *Xenopus laevis* · Interdigital cell death · Developmental acceleration · Mesenchymal cell culture · Webbed-limb formation

Introduction

Cell death is closely related to a variety of biologically important processes such as deletion of unnecessary organs and tissues (Kerr et al. 1974), developmental morphogenesis (Roberts et al. 1999), nervous system development (Roth and D'Sa 2001), establishment of self- and non-self recognition in developing immune system (Sohn et al. 2007), normal adult cell turnover (Lippens et al. 2009), and killing of tumor and virus-infected cells (Brincks et al. 2008; Tesniere et al. 2008).

The interdigital cell death (ICD) is a well-known example of the developmental apoptosis in terrestrial vertebrates. This phenomenon was first discovered as a massive cell degeneration in interdigital mesoderm using avian (chick and duck) embryo (Saunders and Gasseling 1962; Saunders and Fallon 1966) and a concept was established that the morphogenetic roles of ICD are in causing separation of digits through shaping and remodeling the contours of the digital plate (Hinchliffe and Thorogood 1974). About 20 yr later, some amniotic ICD were found to occur under the regulation by a bone morphogenic protein (BMP) signaling (Ganãn et al. 1996; Yokouchi et al. 1996; Zou and Niswander 1996).

Despite their morphogenetic importance, the ICD mechanism is applicable only to amniotic vertebrates such as avian (chick and duck), mammals (rat, mouse, human, etc.), and reptiles (lizard and turtle), but not to amphibians (Cameron and Fallon 1977; Montero and Hurle 2010). This paradoxical situation was originally given from a report by Cameron and Fallon (1977) that vital dye (brilliant cresyl blue or neutral red) staining and histological analysis detected no necrotic zones in

forelimb and hindlimb buds of several amphibians species, i.e., frogs (*Xenopus laevis* and *Bufo americanus*), salamanders (*Ambystoma mexicanum* and *Ambystoma maculatum)* and a newt (*Taricha torasa*). Furthermore, to seek a resolution of the problem that not only hindlimbs (with webbing in adulthood) but also forelimb buts (no webbing in adulthood) of *X. laevis* show no sign of ICD, they measured the DNA synthetic activity of interdigit (ID) and digit (D) mesenchyme parts. They found the forelimb-specific decrease of ID/D growth ratio, and thus provided the idea that free digits in *Xenopus* forelimb develop as a result of differential growth rate between ID and D regions. Furthermore, they subsequently demonstrated the presence of ICDs in turtle and lizard as different amniotic tetrapods other than avian and thus concluded that cell death became an integral part of the formation of free or partially free digits with the emergence of the Amniota, while cell death probably was never a part of free digit formation among the Amphibia (Fallon and Cameron 1977).

Recent studies with mouse limbs revealed that differential growth between digital (D) and interdigital (ID) regions occurs during digit individualization and suggests that the role of ICD is controlling the growth of ID regions and thus allows digits to protrude distally (Salas-Vidal et al. 2001; Hernandez-Martinez and Covarrubias 2011). They proposed two opposing mechanisms for digit separation, one is a classic "massive ICD model" by sculpting function of ICD (as in chicken case) and the other is a new "progressive ICD model" by ICD's growth-limiting function (as in mouse case), and pointed out different contribution of each mechanism among different species. In the present study, we speculated that this model or a version of "progressive ICD model" is applicable to *Xenopus* forelimb individualization because there was a differential growth rate between ID and D regions during their digit development (Cameron and Fallon 1977). Given this perspective, it may be possible that a small amount of cell death is involved in *Xenopus* digit individualization through their roles of "growth-limitation" rather than sculpting function.

It is well established that the BMPs expressed in ID regions are the triggering signals for the ICD of chick and mouse embryos (Guha et al. 2002; Zuzarte-Luis and Hurle 2005). Although *Xenopus* ICD was reported to be undetectable (Cameron and Fallon 1977), a clear-cut BMP-4 expression was observed exactly in the ID regions, as reported by Satoh et al. (2005) and Beck et al. (2006), suggesting the involvement of BMP expression in cell death induction at this regions. Why cannot we detect *Xenopus* ICD? In response to this, we speculated that the undetectable situation of *Xenopus* ICD is the result of their less frequency due to their small size of limb bud and slow developmental speed as compared to chick (or mouse) embryonic development (Hamburger and Hamilton 1951; Nieuwkoop and Faber 1967 Theiler 1989). Furthermore, developmental retardation sometimes occurs in *X. laevis* tadpoles (Nye and Cameron 2005). In this situation, the expected occurrence rate (EOR; see the "Discussion" section) of ICD will further decrease. Taken all together, for the successful detection of *X. laevis* ICD, we have to improve the lower occurrence of *Xenopus* ICD owing to their small ID size, slow developmental speed and individual growth tardiness or variation.

It is well-known that anuran limb growth and differentiation is under direct control of thyroid hormone (Allen 1925; Brown et al. 2005) and administration of thyroxine to tadpoles accelerates the metamorphic events including forelimb and hindlimb growth (Kaltenback 1953). Here, in the present study, we at first tried to accelerate the tadpole development by administration of triiodo-L-thyronine (T_3) in order to improve lower occurrence of *Xenopus* ICD. The second approach we took was a forced induction of ICD by applying BMP-4 to the limb buds. Fortunately, these two trials enabled a relatively good detection of *Xenopus* ICD. For the third trial, we employed cell culture system to quantify the expected difference in ICD occurrence rates between non-webbed forelimbs and webbed hindlimbs of *X. laevis* tadpoles.

Materials and Methods

Animals. Adults of African clawed frog, *X. laevis*, were obtained from local animal suppliers. Fertilized eggs were grown to young frogs in our laboratory at 22–24°C. Tadpoles were staged as described (Nieuwkoop and Faber 1967).

T_3 acceleration of tadpole development. Tadpoles with normal developmental speed among siblings (Nieuwkoop and Faber 1967) were basically used for the experiment (Table 2 and Fig. 1). These tadpoles at stage 53 were selected and divided into control and T_3 groups (7 tadpoles in each group). T_3 (3, 3′, 5-triiodo-L-thyronine; 3×10^{-10} M or 10^{-9} M) were daily added to the T_3 groups after changing water. After 3 d, the forelimbs and hindlimbs were dissected

Figure 1. Effects of developmental-acceleration by T_3 on the number of vital dye-stained cells in *X. laevis* limbbuds. The dye (*neutral red*; NR) staining results were shown in photographs (forelimb: *A1–3* and hindlimb: *B1–3*) and the stage progression during 3 d of T_3 treatment was indicated at the *bottom* of the figures. *A4* (forelimb) and *B4* (hindlimb) are untreated control tadpoles at stage 55. The magnified views of the forelimb interdigit-3 (*A1–4*, *dotted squares*) and hindlimb interdigit-4 (*B1–4*, *dotted squares*) were shown under each photograph (*A1'–4'* and *B1'–4'*, respectively) and the *numbers of NR-stained cells within the squares* were shown at the *bottom*. The quantified results of NR-staining were shown in *C* (forelimb) and *D* (hindlimb). The ordinate shows the number of dye-stained cells and the abscissa shows the concentration of T_3. *Red columns* show the number of stained cells in whole autopod and *blue columns* are those within interdigit-3 or 4.

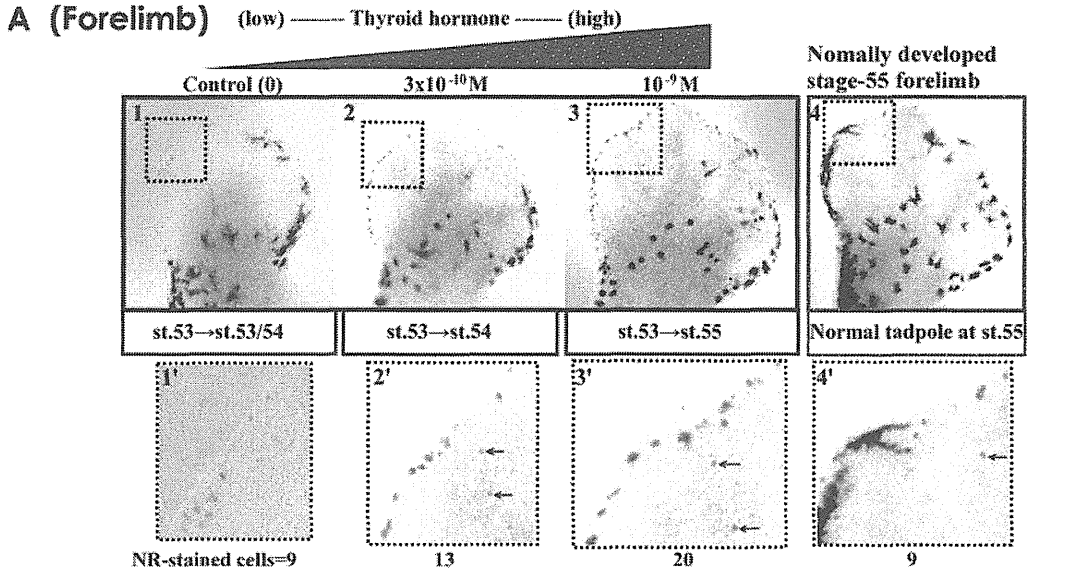
A (Forelimb)
(low) Thyroid hormone (high)
Control (0)
3x10-10M
10-9M
Nomally developed stage-55 forelimb
st.53→st.53/54
st.53→st.54
st.53→st.55
Normal tadpole at st.55
NR-stained cells=9
13
20
9

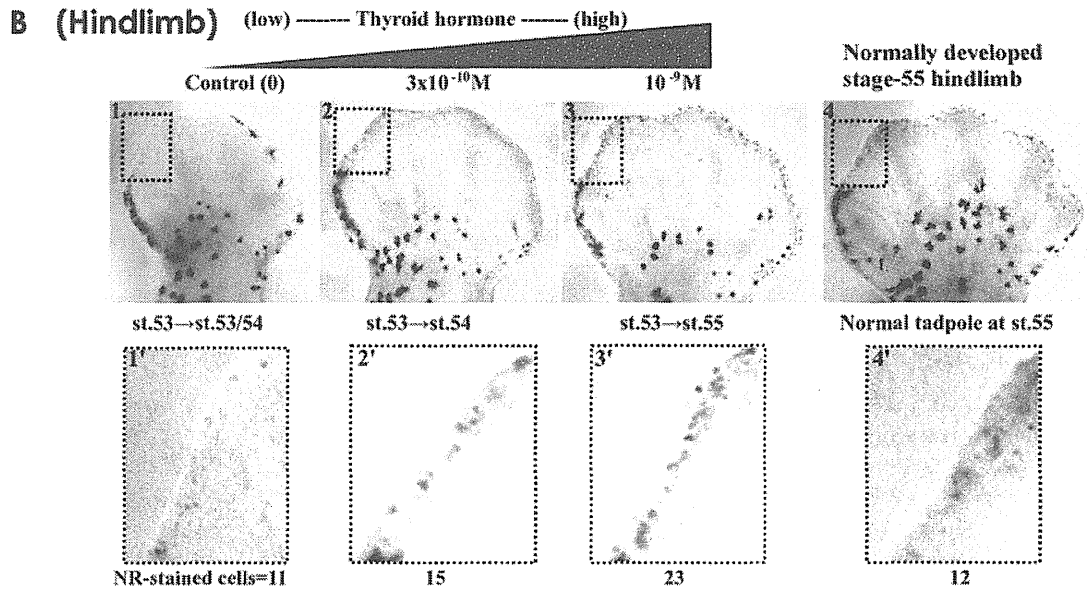
B (Hindlimb)
(low) Thyroid hormone (high)
Control (0)
3x10-10M
10-9M
Normally developed stage-55 hindlimb
st.53→st.53/54
st.53→st.54
st.53→st.55
Normal tadpole at st.55
NR-stained cells=11
15
23
12

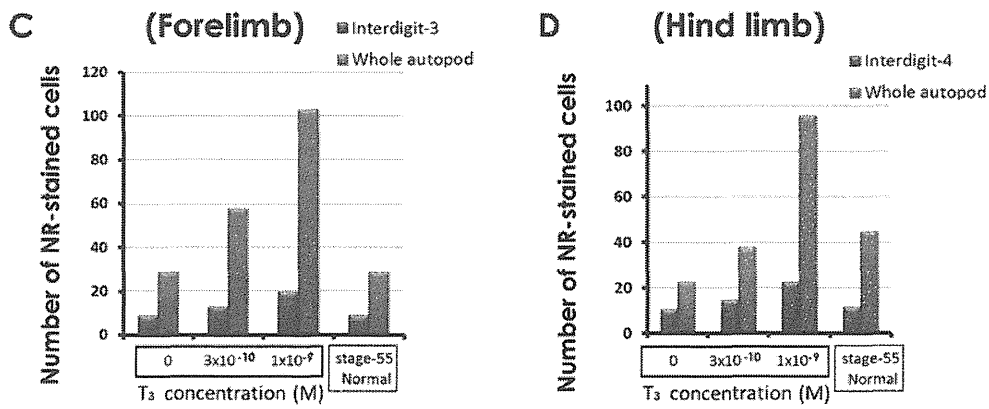
C (Forelimb)
Interdigit-3
Whole autopod
Number of NR-stained cells
120
100
80
60
40
20
0
0
3x10-10
1x10-9
stage-55 Normal
T3 concentration (M)
D (Hind limb)
Interdigit-4
Whole autopod
Number of NR-stained cells
100
80
60
40
20
0
0
3x10-10
1x10-9
stage-55 Normal
T3 concentration (M)

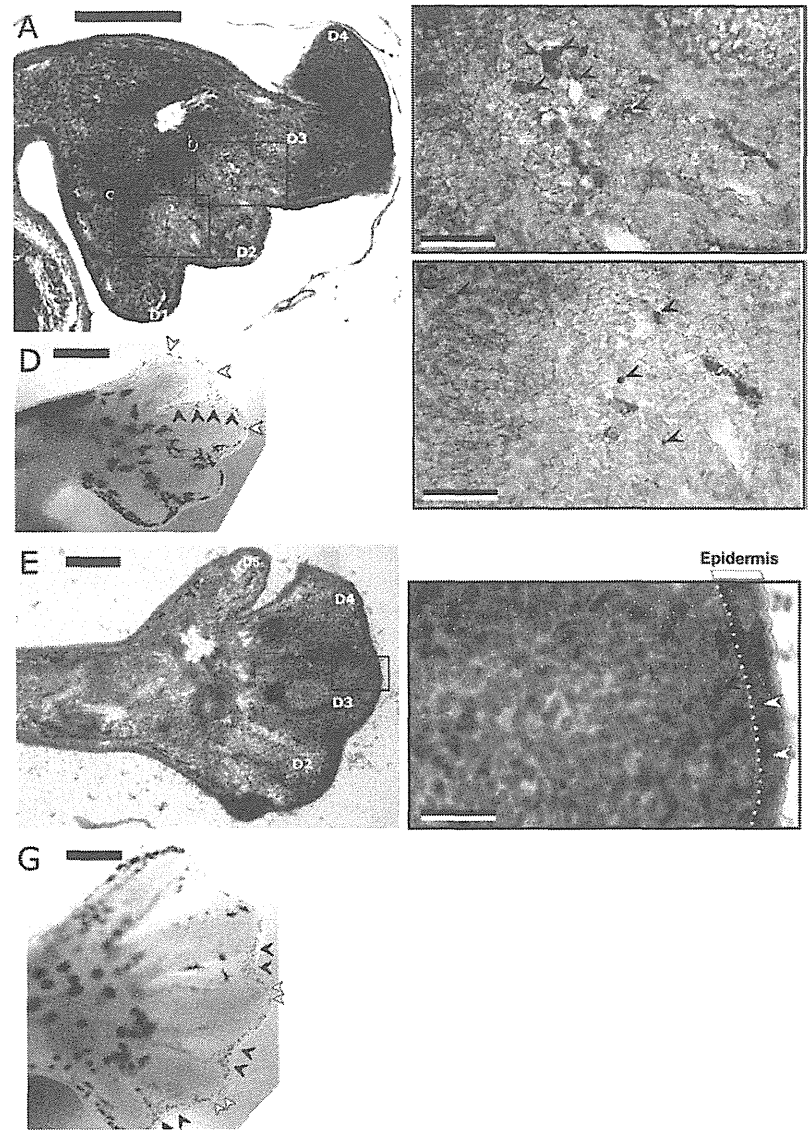

Figure 2. *A*, *B*, *C*, *E*, and *F*: TUNEL-staining of the section of developing limb buds. Paraffin sections of forelimbs (*A–C*) and hindlimbs (*E–F*) of stage-55 *X. laevis* tadpoles were processed for TUNEL reaction. TUNEL$^+$ cells (*red-colored*) at the interdigital mesenchymal regions and epidermal regions are indicated by *black* and *yellow arrowheads*, respectively. *D1–D5*: Digits-1 to -5. The *bars* in *A* and *E* show 0.25 mm. The *bars* in *B*, *C*, and *F* show 0.05 mm. *B*, *C* and *F*: Enlarged figures of *squares b* and *c* in *A* and *square f* in *E*, respectively. *Yellow dot line* in *F* shows the boundary between epidermis and mesenchyme. *D* and *G*: Vital dye (*neutral red*)-stained forelimb and hindlimb of stage-55 tadpoles, respectively. The NR-stained cells in mesenchyme and AER are indicated by *black* and *yellow arrowheads*, respectively. The *bars* in *D* and *G* indicate 0.25 mm.

and processed for vital dye (neutral red) staining (Saunders and Fallon 1966).

Detection of cell death and cartilage nodules. For neutral red (NR) staining, the limb buds of tadpoles were excised and incubated with 3×10^{-4} % of NR in phosphate buffered saline (PBS; 10 mM Na–phosphate buffer, 100 mM NaCl, 1 mM $CaCl_2$, 1 mM $MgCl_2$, pH 7.2) in a petri dish. When the staining was optimal, the samples were washed with PBS. Cell death was also analyzed in vivo sections and in vitro cultures using TUNEL (TdT-mediated dUTP nick end labeling) reaction (Gavrieli et al. 1992). For in vivo analysis (the Fig. 2 experiment), the developing limbs were fixed in 4 % paraformaldehyde (PFA) and embedded in paraffin. TUNEL was performed on de-waxed sections (6 μm) using an "In situ cell death detection kit, AP" (Roche Diagnostics, Mannheim, Germany). Fast Red (Sigma, St. Louis, MO) was used as an alkaline phosphatase substrate. After the reaction, the specimens were counterstained with methyl green. For cultured mesenchymal cells (the experiments in Figs. 4 and 5), they were fixed in 4 % PFA and subjected to TUNEL using "In situ cell death detection kit, POD" (Roche). Diaminobenzidine was used as a peroxidase substrate. After the reaction, the specimens were fixed with 4 % PFA and stained overnight with 1 % alcian blue in 3 % acetic acid, in order to visualize the cartilage nodules.

BMP-4 treatment of dissected limb autopods. Tadpoles at stage 52 were incubated in water containing 10 mM thiourea, a thyroid hormone synthesis inhibitor, for 1 wk. This treatment leads tadpoles to an arrested situation within stage 53/54. After the tadpoles were anesthetized with 0.05 %

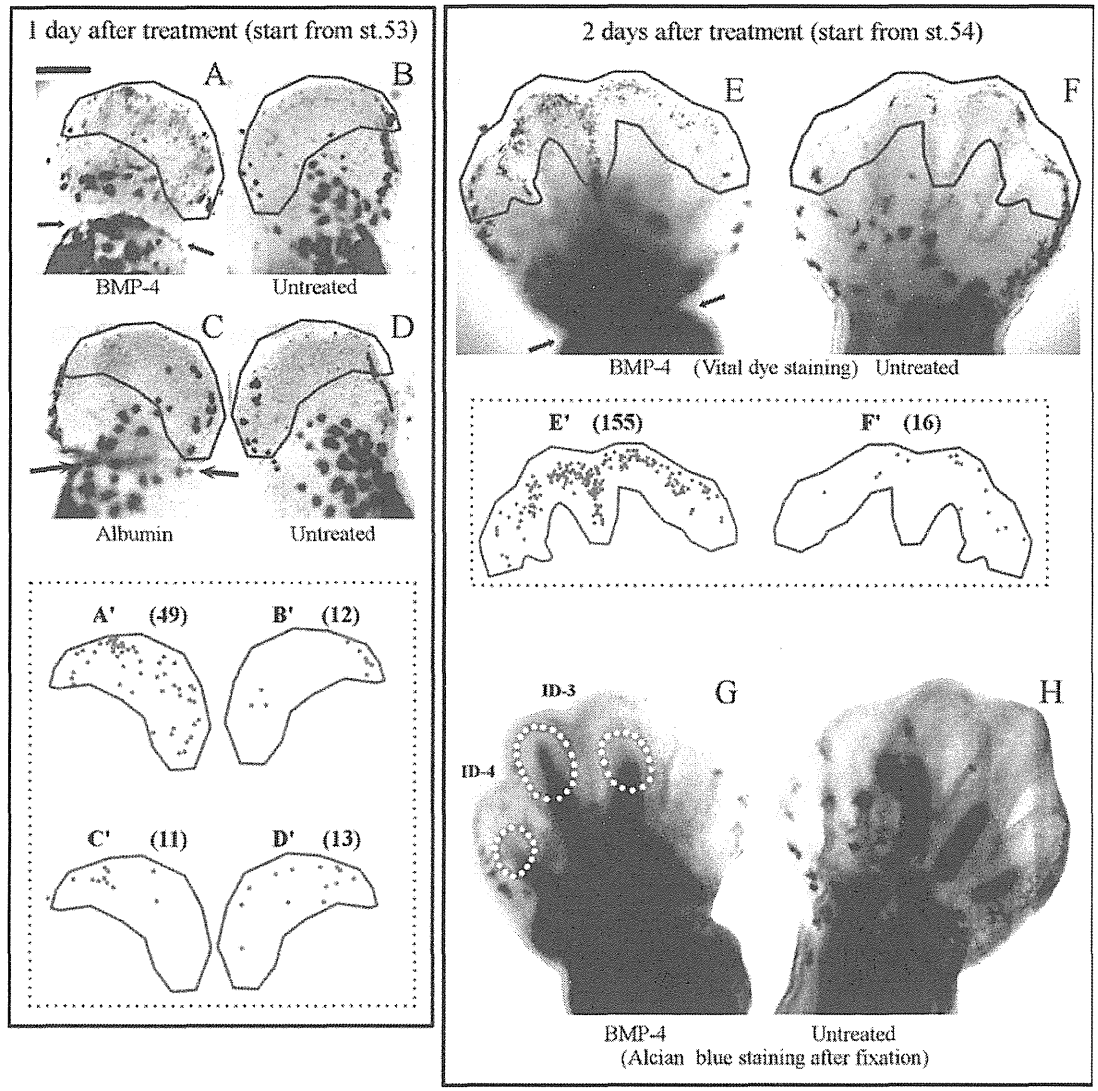

Figure 3. Effects of bone morphogenic protein (BMP)-4 on the number of vital dye-stainable cells and the digital cartilage formation in autopods of stage-53 (*A–D*) and stage-54 (*E–H*) *X. laevis* tadpoles. *A* and *E*: BMP-4-treated left hands. *B*, *D* and *F*: untreated control right hands. *C*, albumin-treated sham control. *Bar* in *A*=0.2 mm. The *arrows* in *A*, *C*, and *E* indicate the position of amputation. The dye-stained cells within areas *enclosed with a red line* on the photographs (*A–F*) were traced and shown in schematic illustrations (*A'–F'*), respectively. The *figures in parenthesis* indicate the number of dye-stained cells in these areas. Figures *G* and *H* show the alcian blue-staining patterns of figures *E* and *F* samples, respectively. The precociously formed digits-3 to -5 are *circled* by the *yellow dot lines* in *G*.

Table 1. Days required for digit formation in various tetrapods

Aminals	Stages	Days after F (or G)[a]	Days required for digit formation	Reference
Gallus domesticus (chick)	27HH–35HH	5–8	3	Hamburger and Hamilton (1951)
Onychodactylus japonicus (salamander)	Stages 53–57 (finger differentiation I–V)	118–148	30	Iwazawa and Kera (1980)
Bufo bufo japonicus (Bufo vulgaris; toad)	Hindlimb formation stages 1–5	21–55	34	Baba and Okada (1932)
Xenopus laevis (frog)	52NF–57NF	21–41	20	Nieuwkoop and Faber (1967)

[a]Days after fertilization (or gestation)

Table 2. T_3 acceleration of *Xenopus laevis* development

T_3 added	Days[a] from stages 52 to forelimb-emergence	Relative developmental speed[b] (fold)
0 (control)	23.8±2.5	1
10^{-9} M	7.1±1.7	3.3

[a] Mean values±S.D. were calculated from 7 tadpoles

[b] The developmental speed of control tadpoles was defined as 1

MS222 (Sigma, St. Louis, MO), the autopod of left hindlimb bud was dissected and soaked for 1 h in 30 % PBS containing 0.3 mg/ml BMP-4 (human recombinant, R & D systems, Minneapolis, MN) or 0.3 mg/ml albumin (bovine serum). The treated autopod was returned to the amputated stump of the same tadpole with a tungsten wire pin (0.02 mm in diameter). The manipulated tadpoles were grown for 1 to 2 d in 30 % PBS with 10 mM thiourea. Pins were removed 1 d after operation.

Alcian blue staining of whole limbs. For skeletal preparation (Fig. 3*G*, *H*), the limbs were fixed with 10 % formaldehyde, washed with acid alcohol (1 % HCl in 70 % ethanol), and then stained with 0.1 % alcian blue in acid alcohol for overnight. After washing with acid alcohol, the specimens were dehydrated with alcohol and cleared with methyl salicylate.

Micromass culture of limb mesenchymal cells. Cell death and chondrogenesis of *Xenopus* limb mesenchyme were analyzed in vitro with high density micromass culture technique as described (Daniels et al. 1996) with following modifications. All media used for cell culture were diluted to 70 % strength. Limb buds were dissected and treated with 0.25 % trypsin–0.2 % collagenase for 2 h at 27°C. Dissociated cells were passed through three-layered lens cleaning tissue (Whatman, Maidstone, England). This filtration process could almost totally remove the epidermal tissues. The extent of contamination by epidermal cells was checked by immunostaining of low density (2.5×10^4 cell/5-mm well) cultures of isolated cells using anti-pan-cytokeratin monoclonal antibody (clone C-11, Sigma-Aldrich, St. Louis, MO) and found to be below 0.1 % (Fig. 5*J*, *K*). The number of mesenchymal cells isolated from one limb was ~6×10^4 cells (stage 53; forelimb) or 12×10^4 cells (stage 53; hindlimb). The number of tadpoles pooled for one experiment was 25 for forelimb cultures and 13 for hindlimb cultures. The cell concentration was adjusted to 1×10^7 cells/ml and the cells were placed as 10 µl drops (1×10^5 cells/well) in the center of each well of a 24-well tissue culture plate. After 2 h, the wells were filled with Ham's F-12 medium (diluted with dH_2O to 70 % strength) supplemented with 10 % resin-treated serum (RTS). RTS was made by treating fetal calf serum with AG1-X8 resin (Bio-Rad, Hercules, CA) to remove T_3 (Samuels et al. 1979). The cultures were incubated at 25°C under 5 % CO_2/95 % air in humidified condition and added with (or without) T_3 (10^{-8} M) 1 d after inoculation. The culture medium was changed every 2 d.

Results

T_3 accelerated the tadpole's development and enabled a better detection of vital dye-stainable cells. First of all, we investigated bibliographically how the speed of digital development is different between amphibians and amniotes (Table 1). The days required for digit formation in chick and mouse (amniotes) are about 3 d (Hamburger and Hamilton 1951; Theiler 1989), while those for amphibians take much longer times: *Onychodactylus japonicus* (salamander) 30 d (ten times longer; Iwazawa and Kera 1980), *Bufo bufo japonicus* (toad) 34 d (eleven times longer; Baba and Okada 1932), and *X. laevis* (frog) 20 d (seven times longer, Nieuwkoop and Faber 1967).

In order to see if triiodo-L-thyronine (T_3) really accelerates the speed of digital development in *X. laevis*, the times required from stage 52 to forelimb emergence were measured for the tadpoles incubated with or without T_3 (Table 2). Control tadpoles (without hormone) required 23 d for the process, while tadpoles with T_3 (10^{-9} M) required only 7 d (about 3-fold acceleration).

Using the T_3-accelerated *X. laevis* tadpoles, vital dye staining was conducted (Fig. 1). Tadpoles at stage 53 were divided into 3 groups and incubated in tap water with T_3 (3×10^{-10} M or 10^{-9} M) or without T_3 (control). After 3 d, tadpole's stages were judged and their limbs were dissected for vital dye (neutral red) staining assay. Without T_3 (control group), tadpole's stage became 53/54 and vital dye-stained few (9–11 or below) cells within an interdigital space (ID-3 of forelimb or ID-4 hindlimb) as very faint spots, being consistent with a hard-to-find nature of *Xenopus* ICD. In a tadpole group with 3×10^{-10} M T_3 (stage 54), the size of vital dye-stained cells appeared to be large and the number of stained cells increased to 13–15 (1.5-fold). In a tadpole group with 10^{-9} M T_3 (stage 55), the size of stained cells became much larger and the number increased further to 20–23 (2- to 3-fold; Fig.1*A*, *B*). Most of stained cells were distributed around distal margin of the autopods, but some stained cells (indicated by arrows in *A2'–4'*) were observed in proximal interdigital spaces only in forelimbs (but not in hindlimbs). Throughout the whole autopod the total number of stained cells increased 2- or 4-fold by addition of 3×10^{-10} M or 10^{-9} M T_3, respectively (Fig.1*C* and *D*). These results demonstrated that addition of T_3 to *X. laevis* tadpoles improved the expected occurrence rate (EOR) of ICD and enabled a better detection of vital dye-stainable cells.

Next, we examined whether dying cells can be detected in interdigital regions by the other method (i.e., TUNEL reaction using limbbud sections) than vital dye staining in order to clarify the relation between the vital dye-stained cells and the detection of *Xenopus* ICD (Fig. 2). The TUNEL reaction was a widely used reliable method for detecting apoptotic cells based on the DNA nick-end labeling (Gavrieli et al 1992). The results showed the $TUNEL^+$ dying cells with DNA breakages were observed in the central (or proximal) part of the forelimb interdigital regions (Fig. 2*A–C*) and the distal part of the hindlimb interdigits and AER (apical ectodermal ridge; Fig. 2*E*, *F*). This distribution pattern of $TUNEL^+$ cells was essentially consistent with that of vital dye-stained cells (Figs.1 and 2*D*, *G*). Furthermore, the $TUNEL^+$ dying cells were found both in mesenchyme (Fig. 2*B*, *C*, *F*, black arrowheads) and epidermis (AER; Fig. 2*F*, yellow arrowheads) and these points also agreed the results in vital dye staining (Fig. 2*D*, *G*). This spatial coincidence between patterns of vital dye and TUNEL staining confirms that it is really possible to detect ICD by vital dye staining in *Xenopus* limbbuds.

Excess application of BMP-4 enhanced digital cartilage formation and increased the number of vital dye-stainable cells in X. laevis autopods. In order to improve an EOR of *Xenopus* ICD, BMP-4 which is one of the powerful inducer of amniotic ICD was added locally to the autopods of tadpoles at stages 53 and 54 (Fig. 3). The autopods were dissected, soaked in a solution containing human recombinant BMP-4 (0.3 mg/ml) for 1 h, and repositioned to their original limb stamps with thin pin wires (0.02 mm in diameter).

Figure 3*A* shows the vital dye (neutral red) staining of a left hand of tadpoles (stage 53) 1 d after BMP treatment. The number of vital dye-stained cells in a BMP-treated autopod increased 4-fold as compared with that in untreated control right hand (BMP/control=49 cells:12 cells). As a negative control, an albumin solution (Fig. 3*C*) was added instead of BMP but the stained cell ratio was not changed.

Figure 3*E* shows the vital dye staining of an autopod (a left hand of tadpoles at stage 55) 2 d after BMP treatment. The number of vital dye-stained cells in BMP-treated autopod increased 10-fold as compared with that in untreated control (a right hand; BMP/control=155 cells:16 cells). These samples (*E* and *F*) were fixed and stained with alcian blue in order to detect their digital cartilage patterns (Fig.3*G* and *H*, respectively). Application of BMP-4 induced the precocious formation of digits-3 to 5 (Fig. 3*G*; enclosed with yellow dot circles). More than 60 % of vital dye-stained cells was distributed between BMP-induced digital cartilages (ID-3 and -4). These results indicated that addition of BMP-4 to developing autopods improved the EOR of *Xenopus* ICD and enabled a better detection of vital dye-stainable cells.

Cell culture technique application for the detection of Xenopus ICD. In order to make cell death detection highly efficient and quantitative, mesenchymal cells were isolated from *X. laevis* limb buds, cultured in a plastic plate at a high density (10^5 cells/10 μl drops) in manner of micromass culture (Daniels et al. 1996) for 6 d, and assayed for cell death (TUNEL method) and also chondrogenic activities (alcian blue staining of cartilage nodules; Figs. 4 and 5).

At first, in order to confirm whether the isolated cells are indeed mesenchymal (Yokoyama et al 1998), extent of contamination by epidermal cells was examined by using pan-cytokeratin-immunostaining (Figs. 5*H–K*). Figure 5*H*, *I* shows the keratin-immunostaining of a culture (1 d after inoculation) of the hindlimb cells isolated without lens paper filtration. In this case, keratin-positive epidermal cells (brown color, arrows in *H* and *I*) were observed as small cell aggregates which consist of 20–50 cells and the area occupied by these epidermal aggregates was about 1 % of total culture area. In contrast, the aggregate size became smaller (3–10 cells) and the epidermal area was reduced to below 0.1 % when the cell isolation was done with lens paper filtration (Fig. 5*J*, *K*), indicating that the filtration process is effective for yielding high purity (99.9 %) of mesenchymal cells. For the forelimb cells, almost the same purity of mesenchymal cells was achieved (not shown). Therefore, it is conceivable that there is no serious effect of epidermal cells on the assays for cell death and chondrogenic activities of mesenchymal cells. Using these mesenchymal cells, we applied micromass culture technique for the assay of cell death and chondrogenic activities (Figs.4*A–G* and 5*A–G*).

In forelimb-cell cultures, TUNEL-positive dying cells (brown-colored cells with DNA breakages indicated by red arrowheads in Fig. 4*A–E*) were observed in control condition (w/o T_3) from the 1st day of culture and their number did not increase during 6 d. In the presence of T_3, the dying cell number increased 2-fold (Fig. 4*D–F*). Since the cartilage tissues are known to be important for induction of chicken ICD (Omi et al. 2000), the cartilage induction was examined in *X. laevis* cell cultures. In control forelimb-cell culture, the cartilage nodules (yellow asterisks) were slightly formed (20 nodules/well) during 6 d, while they were formed rapidly and massively (176 nodules/well) in T_3 cultures (Fig. 4*E*, *G*).

In hindlimb-cell cultures, TUNEL-positive dying cells were observed in control cultures from the 1st day but their number did not increase throughout the culture period (Fig. 5*A–C* and *F*). In the presence of T_3, a small increase (1.25-fold) in $TUNEL^+$ cell number was observed during the early short time of culture (Days 1–4; Fig. 5*D*, *F*). The cartilage nodules were not formed in control hindlimb-cell cultures but formed gradually (65 nodules/well) in the presence of T_3 at a rate slower than that in forelimb cultures with T_3 (Fig. 5*A–E*, *G*).

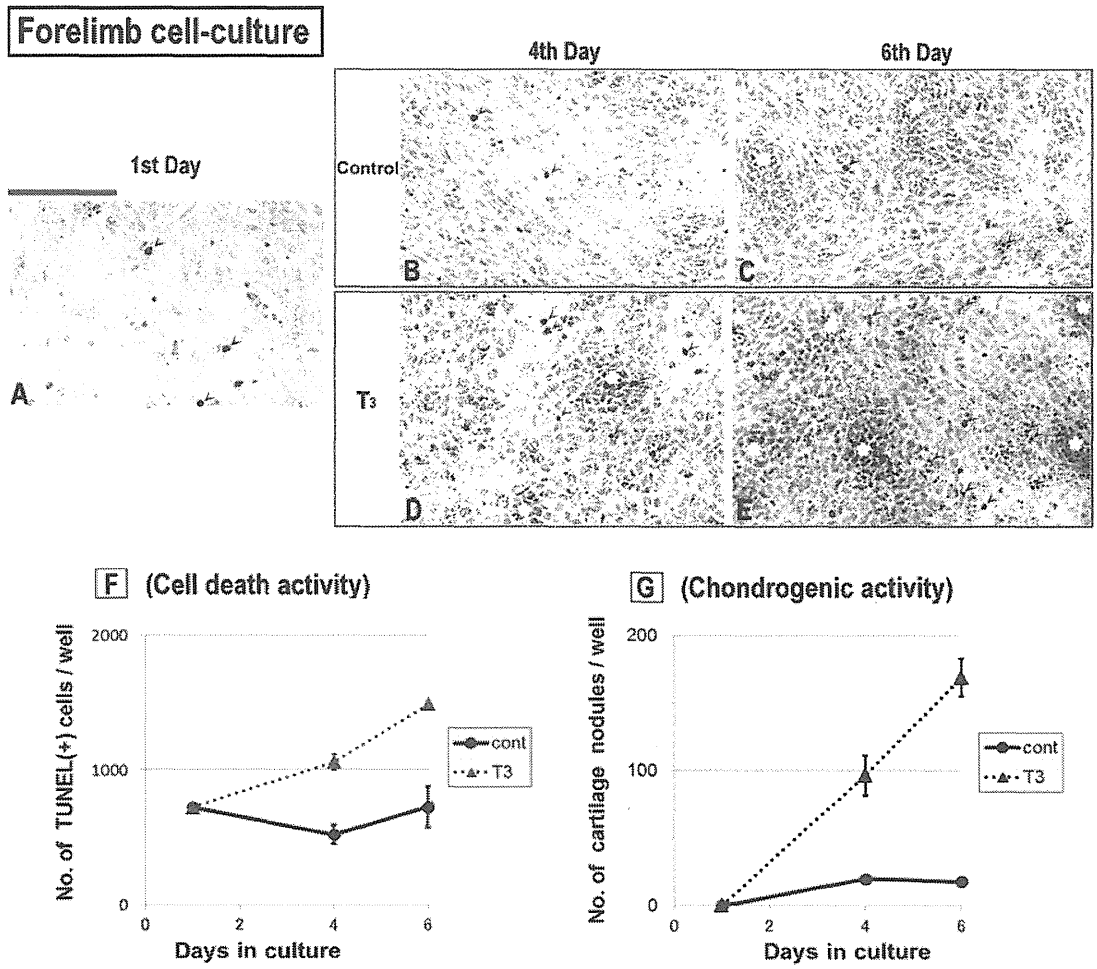

Figure 4. Detection of cell death and chondrogenic activities in cultured mesenchymal cells isolated from forelimbs of stage-53 *X. laevis* tadpoles. *A–E*: Photomicrographs of cultured cells stained with alcian blue and TUNEL. After the first day, the cultures were added with T_3 (10^{-8} M; T_3, *D* and *E*) or not (control; *B* and *C*). The *red arrowheads* indicate $TUNEL^+$ cell (*brown-colored*) and the *yellow asterisks* indicate cartilage nodules. The *bar* in *A*=0.1 mm. *F*: Quantification of $TUNEL^+$ cells. The ordinate shows the number of $TUNEL^+$ cells per well (*red triangles*=T_3; *black circles*=control). The abscissa shows the days in culture. *G*: Quantification of chondrogenic activity by counting of cartilage nodules. The ordinate shows the number of cartilage nodules per well (*blue triangles*=T_3; *black circles*=control). The abscissa shows the d in culture. *F* and *G*: For all points, the mean values from two wells are shown with their range (*vertical lines*). Several experiments were conducted and similar results were obtained.

These results showed that cell culture technique can be used for efficient and quantitative detection of limb mesenchymal cell death in *X. laevis* and that T_3 enhances the cell death and chondrogenic activities. Furthermore, the T_3 enhancement was much stronger in forelimb cells than in hindlimb cells.

Discussion

The expected occurrence rate (EOR) of ICD is very low in X. laevis. We speculated that the undetectable *Xenopus* ICD is due to far less occurrence of ICD in *Xenopus* than in chick or mouse. The speculation is based on the following calculation. (1) The width of *Xenopus* limb bud is one third times smaller than that of chick at comparable stages (i.e., 0.3 mm vs. 1 mm), so that the area within one interdigit (ID) of *Xenopus* limb bud is about one ninth smaller than that of chick one. (2) The *X. laevis* digit formation progresses more slowly than the chick one. Digit formation process in *X. laevis* (from stage 52 to 57) requires a 7 times-longer period (20 d) than that in chick (about 3 d). (3) From 1 and 2, the expected occurrence rate (EOR) of ICD in *X. laevis* in comparison with the chicken case is calculated as follows:

$$\begin{aligned}(\textbf{EOR of } \textit{Xenopus} \textbf{ ICD}) &= (\textbf{small size factor}) \times (\textbf{slow speed factor}) \\ &= 1/9 \times 1/7 \\ &= 1/63\end{aligned}$$

If some technique (e.g., vital dye staining) detect 400 dying cells within one chicken ID, the same technique will detect,

with this formula, only 6 dying cells (i.e., $400 \times 1/63 \approx 6.35$) within one *X. laevis* ID. (4) Furthermore, spontaneous developmental retardation sometimes occurs in *X. laevis* tadpoles. For example, normal tadpoles progress within 3 d from stage 55 to 56, during which obvious digit individualization occur, while developmentally delayed tadpoles requires around 2 wk for the same process (Nye and Cameron 2005). In this situation, the expected cell death number in one ID will decreases even to one to two cells in calculation. Thus, it is conceivable that the main reason for undetectable situation of *Xenopus* ICD is involved in far less occurrence of ICD.

T_3 acceleration of developmental speed is effective for the detection of Xenopus ICD. The most important result in the present study was a finding of the availability of acceleration of developmental speed for the detection of *Xenopus* ICD. We found that addition of T_3 to tadpoles improved the appearance rate of *Xenopus* ICD and enabled a better detection of vital dye-stainable cells. In normal tadpoles without T_3 addition, the EOR of *Xenopus* ICD was very low in calculation and indeed very few (or almost no) vital dye-stained cells were observed in the limb buds (Fig. 1*A*, *B* control), which was consistent with the original report by Cameron and Fallon (1977). Therefore, it is reasonable to accept the idea that ICD does not occur in *X. laevis* tadpoles in the circumstances of their slow-motion type normal development. However, in developmentally accelerated condition by T_3 (three times faster than normal speed; Table 2), the occurrence rate of ICD increased 3-fold and a fairly good number of vital dye-stained cells were observed (Fig.1*C*, *D*). This means that successful detection of *Xenopus* ICD is achieved to some extent by the acceleration of developmental speed and suggests some contribution of ICD to the digit-formation process even in *X. laevis*.

Generally, the limb formation in amphibian does progress more slowly than that in amniotes (Table 1). Because of this, observations of amphibian limb events in normal speed often lead to an intuitive judgment that "there is no cell death during limb morphogenesis". If we observe only a few (below 10 cells) vital dye-stained cells (dying cells) in one examination sample, we cannot clear up the doubt that it occurs within the margin of error. In order to recognize the amphibian limb-cell death as a "massive cell death," it is necessary to improve a lower occurrence rate of limb-cell death by accelerating the developmental speed with an appropriate method. Acceleration by thyroid hormone treatment was successfully used in clear detection of ICD. This is because *Xenopus* limb formation process is entirely dependent on thyroid hormone upregulation in vivo. This is easily understood from the fact that tadpoles which are treated with a thyroid hormone-synthesis inhibitor (e.g., thiourea and methimazole) before limb-forming stages cannot pass through the digit-forming stages (our preliminary results; Brown et al. 2005). In the present study, acceleration of T_3-dependent process by adding T_3 raised cell death frequency (number of occurrence per unit of time) and led to a better situation in detecting vital dye-stainable cells in developing limbs of *X. laevis*.

We also clarified that dying cells with DNA breakage ($TUNEL^+$ cells) was really present in the vital dye-stained area (Fig. 2). Furthermore, the $TUNEL^+$ dying cells were found both in mesenchyme and epidermis and these points were consistent with the results in vital dye staining (Figs.1 and 2*D*, *G*). However, it is unknown what the types of dying mesenchymal cells are and how these dying cells are processed by phagocytosis. From these points of view, further characterization of *Xenopus* ICD remains as a future important work.

Is the action of T_3 on Xenopus ICD identical to that on larval organ-specific apoptosis during anuran metamorphosis? Is there a possibility that ICD is induced by the other function of T_3 than the growth-stimulating function through the upregulation of basal metabolism? To answer this question, a great deal of consideration should be given to the fact that T_3 has a prominent function as an apoptotic cell death inducer for the larval-specific organs during anuran metamorphosis. By studies using bullfrog larval epidermal cells (Nishikawa and Yoshizato 1986; Nishikawa et al. 1989) and *Xenopus* myoblasts (Shibota et al. 2000), the major T_3 effects on larval type organ (i.e., tail cells) were found to be following three points: (1) inhibitoin of cell cycle progression, (2) induction of apoptosis of larval cells, and (3) inhibition of cell differentiation. Furthermore, the induction of rapid cell loss and massive apoptotic cell death needed a high dose of T_3 ($\geq 10^{-8}$ M). On the other hand, these effects (1–3) were not observed for the adult type cells (i.e., limb myoblasts); rather, the opposite effect, promotion of cell differentiation, was observed at wide range of T_3 (10^{-10}–10^{-8} M) for the adult myoblasts. This effect was found to be the acceleration of differentiation (early induction: i.e., the days required for myotubes formation was shorten) but not the increase in the number of finally differentiated cells (Shibota et al. 2000).

The digits are the part of limbs which belong to adult but not larval organs, and the digit formation and individualization occur during the early metamorphic period when the T_3 concentration is low-medium levels. Therefore, it seems reasonable that the T_3 actions which direct the ICD is not equivalent to those in "the deletion mechanism (D-mechanism)" of larval organ such as tail at only high T_3 level (10^{-8} M), but rather related to "the promotion mechanism (P-mechanism)" of adult organ differentiation through metabolic acceleration at wide range of T_3 levels (10^{-10}–10^{-8} M). In fact, in the present study, T_3 promoted the ICD occurrence rate at wide range of T_3 concentrations (3×10^{-10}–10^{-8} M; Figs. 1, 4, and 5), suggesting the involvement of "P-mechanism" in *X. laevis* ICD.

BMP-4 application is effective for the detection of Xenopus ICD. In the present study, application of BMP-4 to the autopod was also found to very helpful for detecting vital dye-stainable cells at high density in limb buds of *X. laevis*. In the limb buds without BMP-4 application, the occurrence rate of *Xenopus* ICD is very low. However, in the limb buds soaked with BMP-4, the occurrence rate increased 4-fold at 1st day and 10-fold at 2nd day. It is conceivable that this is due to simultaneously triggered cell death reaction by absorbing high dose of BMP-4 into the mesenchymal cells. In case of mouse limb bud organ-culture, BMP-4 application induced cell death at 0.1 μg/ml (Tang et al. 2000), while the BMP concentration in the present study (0.3 mg/ml) is 3,000-fold higher than that in mouse case. The reason why we employed relatively high concentration (0.3 mg/ml) was because BMP concentration passing through the limb epidermis might come down during treatment of dissected autopod with BMP. This concentration was originally determined by reference to implantation experiments with BMP-soaked beads in which the concentrations of 0.1–2.0 mg/ml of BMPs were effective for the cell death induction and cartilage thickening (Macias et al. 1997). In this and our experiments, there was no notable effect other than induction of cell death and chondrogenic alterations. Therefore, this level of BMP concentration is considered appropriate for the experimental induction (or enhancement) of cell death activity in limbbuds.

The BMP-4 application also had another important effect of earlier induction of digital cartilage differentiation (Fig. 3*G*). Interestingly, more vital dye-stained cells were observed in the region between BMP-induced digital cartilages. This situation is in good agreement with the data pertaining to the requirement of digits for the induction of mouse ICD by BMP (Tang et al. 2000) and positive-relationship between ICD-occurrence and digital cartilage-formation in chick (Omi et al. 2000).

In studies with chicken or mouse limb morphogenesis, the BMP's cell death-inducing effect was often assayed by implantation of BMP-soaked beads into limb bud-mesenchymes (Ganãn et al. 1996; Tang et al. 2000). However, in case of *X. laevis*, the limb-tissue size is too small to undergo beads implantation and thus we employed a simple BMP-soaking method in which dissected limb autopods were soaked directly in BMP solution for 1 h and thereafter returned to the original stumps. Although this method cannot limit the extent of BMP's effects to a small region, we could roughly analyze the BMP's effects on *Xenopus* ICD and cartilage formation by comparing a BMP-treated left limb with a control (untreated) right limb in the same tadpole.

This soaking method with whole autopod was also applicable to an analysis of local T_3 effects. If the dissected limb bud autopods were soaked in T_3 solution and returned to the original stumps, the treated autopods became larger in their sizes and showed more vital dye-stained cells than their control counterparts (data not shown). To put it plainly, acceleration of cell death by T_3 occurs in connection with limb size increase. This is because T_3 acts as a transcriptional master switch for total limb bud differentiation (Das et al. 2006). On the other hand, BMP-4 affects only on cell death and chondrogenic processes without increasing autopod size. Thus, it is conceivable that autopodial BMP-4 signaling lies downstream of the thyroid hormone signal. From this standpoint, it is an important issue to examine whether T_3 regulates the expression of autopodial BMP-4 and/or BMP-inhibitors such as gremlin (Bardot et al. 2004) during prometamorphosis (or limb-growing stage) of *X. laevis*.

Figure 5. Detection of cell death and chondrogenic activities in cultured mesenchymal cells isolated from hindlimbs of stage-53 *X. laevis* tadpoles. *A–E*: Photomicrographs of cultured cells stained with alcian blue and TUNEL. After the first day, the cultures were added with T_3 (10^{-8} M; T_3, *D* and *E*) or not (control; *B* and *C*). The *red arrowheads* indicate $TUNEL^+$ cell (*brown-colored*) and the *yellow asterisks* indicate cartilage nodules. The *bar* in A=0.1 mm. *F* and *G*: Quantification of $TUNEL^+$ cells and chondrogenic activity, respectively. The manner of presentation of the graphic data is the same as in Fig. 4. *H–K*: Evaluation of epidermal contamination during cell separation steps. Hindlimb cells prepared without (*H*, *I*) or with lens paper filtration (*J*, *K*) were immunostained at first day of culture with an anti-pan-cytokeratin antibody. *Red arrows* keratin-positive epidermal cells (*brown-colored*). *Bars*=0.1 mm. *I* and *K*: Magnified figures of the boxed areas in *H* and *J*, respectively.

Cell culture technique is available to assess the quantitative characterization of cell death and chondrogenic activities in X. laevis. Acceleration of metamorphosis (or development) in *X. laevis* tadpoles by T_3 helps us to detect ICD (Fig. 1). Application of cell death inducer (BMP-4) triggers autopodial cell death all at once (Fig. 3). From these situations, it is reasonable that *Xenopus* ICD actually occurs very slowly but it is difficult to be found at the first face. If this is the case, it may be possible to associate the progressive (or low) ICD activity in *X. laevis* with their interdigital webbing formation as described in mouse case (progressive ICD model; Hernández-Martinez and Covarrubias 2011). In order to test this possibility, we planned to quantify ICD activities of both forelimbs and hindlimbs and to demonstrate that ICD activity in the former is much stronger than that in the latter, because there are interdigital webbings in hindlimbs but not in forelimbs in *X. laevis*. We choose a micromass culture system for this aim for the following reasons.

The 3-D culture systems such as collagen gel cultures (Togo et al. 2011), hydrogel 3-D matrix cultures (Kim et al. 2011), "pellet" cultures (Tallheden et al. 2004), and micromass cultures (Ahrens et al. 1977) have been developed for facilitating the in vitro differentiation of mesenchymal cells. Among these, micromass culture is well suited for allowing the cartilaginous differentiation of limbbud mesenchymal

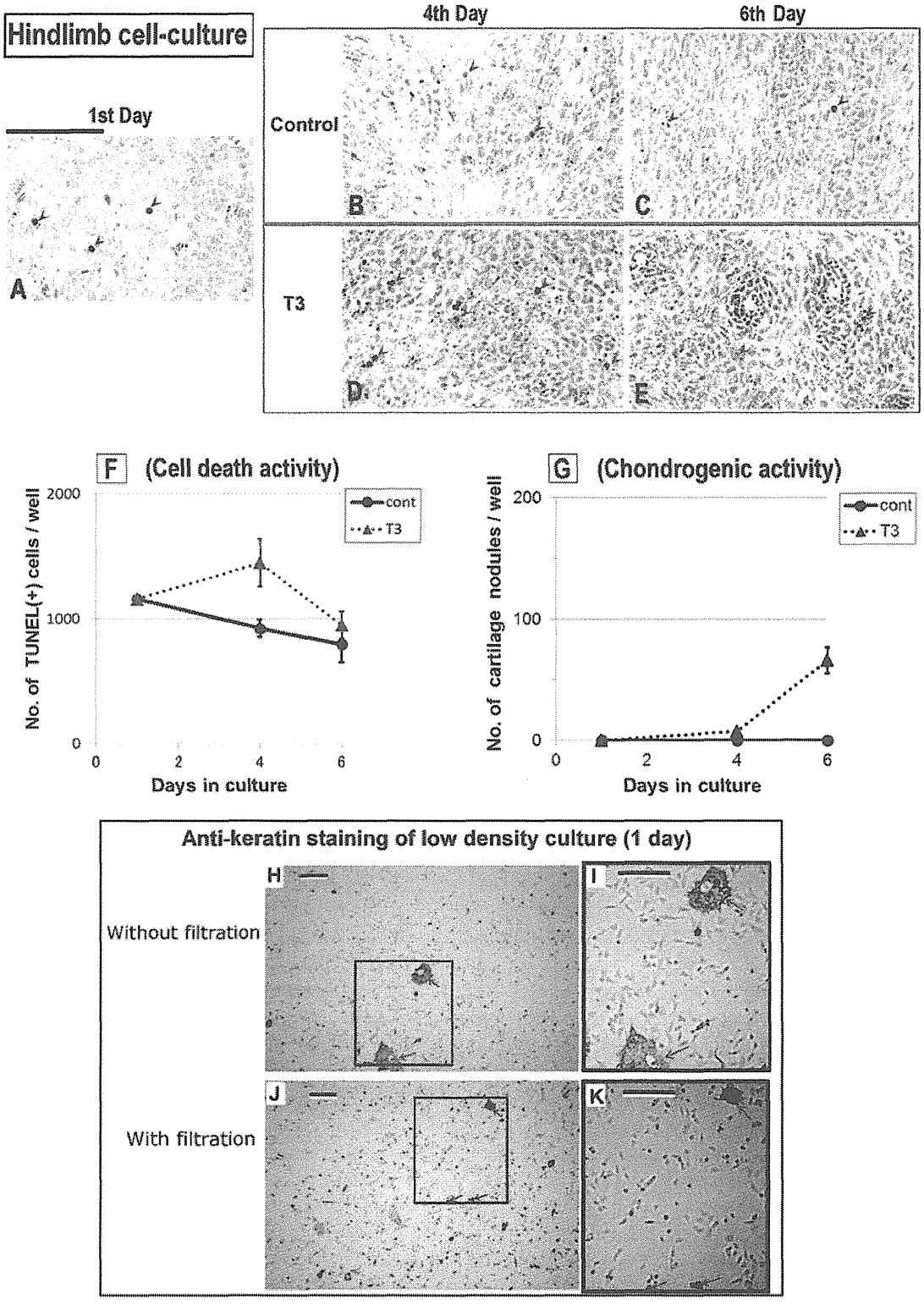

cells (Ahrens et al. 1977) and constructing the 3-D cartilaginous structures (Denker et al. 1995). So, we applied the micromass culture system to *Xenopus* limbbud mesenchymal cell in order to compare ICD and chondrogenic activities between forelimbs and hindlimbs. Actually, in the micromass cultures of *Xenopus* limb cells (Figs. 4 and 5),

the aggregated structures of chondrogenic nodules were formed and cell deaths in inter-nodule spaces were induced during culture period with (or without) T_3. This culture method was thus found to be suited for allowing the differentiation and ICD of *Xenopus* limb mesenchymal cells in vitro. At the same time, a number of $TUNEL^+$ cells (dying cells) were observed in control cultures. These ratios (number of $TUNEL^+$ cells/attached cells × 100 %) were found to be about 1–3 % in forelimb control cultures and about 1–2 % in hindlimb control cultures by the estimation of cell-to-substrate adhesion activity at 1st day after inoculation (>60 % in both cultures; not shown). If we apply the "pellet" culture system (Tallheden et al. 2004) to *Xenopus* limb mesenchymal cells, the death activity in control cultures (1–3 % or 1–2 %) may be minimized. Because, expressions of apoptosis related genes (e.g., *caspase 3*) were significantly downregulated in 3-D "pellet" culture of human articular chondrocytes.

By using micromass culture system and a DNA-nick end labeling (TUNEL), we quantified the cell death activity in *Xenopus* limbbud cells. As a result, it was revealed that the augmentation of cell death activity by T_3 was stronger in the forelimb mesenchymal cells than in the hindlimb cells and period of cell death enhancement by T_3 was longer in the forelimb cells than in the hindlimb cells (compare Figs. 4*F* with 5F). These results indicate that the presence (or absence) of interdigital webbings in hindlimb (or forelimb) might be explained by their differential cell death activities. In essence, more forelimb mesenchymal cells are to die easily and respond strongly to T_3 when compared to hindlimb cells. This quantitative evaluation of ICD with cell culture technique suggest that vital dye staining of autopodial cells is not merely a background error but is a "programmed cell death" which serves in the role of establishing *Xenopus* forelimb or hindlimb morphology.

Cell culture system in the present study was also available not only for cell death analysis but also for quantification of chondrogenic activities (Figs. 4*G* and 5*G*). The chondrogenic activity in the forelimb cells was stronger than that in the hindlimb cells. And the extent of their hormonal enhancement was much greater in forelimb cells than in hindlimb cells. Then, a question arises. Do forelimb webbings disappear due to complete loss of web-forming precursor cell in the forelimb buds by their intense activities of both cell death and cell-recruitment for chondrogenesis? Or are there no such precursor cells from the beginning only in the forelimb buds? In order to solve this question, it is a worthwhile trial to examine whether inhibition of cell death in the forelimb by BrdU treatment causes the web-formation in the forelimbs. The reason for this is that inhibition of chick hindlimb apoptosis with BrdU treatment resulted in web-like structures in their legs (Tone et al. 1983). In this respect, it still remains an important issue for the tetrapod-evolutional biology to closely examine whether there are common mechanisms of cell death and web-differentiation between amniotes and anuran (or urodele) amphibian (Fallon and Cameron 1977).

Acknowledgments This work was supported in part by a Grant-in-Aid for Scientific Research from the Ministry of Education, Culture, Sports, Science, and Technology of Japan. The authors express their thanks to Dr. Naoyuki Wada (Kawasaki Medical School) for his helpful advice on BMP application techniques.

References

Ahrens P. B.; Solursh M.; Reiter R. S. Stage-related capacity for limb chondrogenesis in cell culture. *Dev Biol* 60: 69–82; 1977.

Allen B. M. The effects of extirpation of the thyroid and pituitary glands upon the limb development of anuran. *J Exp Zool* 42: 13–30; 1925.

Baba K.; Okada Y. Frog development (*Bufo vulgaris*). ("Kaeru hassei" in Japanese). Iwanami Publishing Co, Tokyo; 1932.

Bardot B.; Lecoin L.; Fliniaux I.; Huillard E.; Marx M.; Viallet J. P. Drm/Gremlin, a BMP antagonist, defines the interbud region during feather development. *Int J Dev Biol* 48: 149–156; 2004. doi:10.1387/ijdb.041804bb.

Beck C. W.; Christen B.; Barker D.; Slack J. M. Temporal requirement for bone morphogenetic proteins in regeneration of the tail and limb of *Xenopus* tadpoles. *Mech Dev* 123: 674–688; 2006. doi:10.1016/j.mod.2006.07.001.

Brincks E. L.; Kucaba T. A.; Legge K. L.; Griffith T. S. Influenza-induced expression of functional tumor necrosis factor-related apoptosis-inducing ligand on human peripheral blood mononuclear cells. *Hum Immunol* 69: 634–646; 2008. doi:10.1016/j.humimm.2008.07.012.

Brown D. D.; Cai L.; Das B.; Marsh-Armstrong N.; Schreiber A. M.; Juste R. Thyroid hormone controls multiple independent programs required for limb development in *Xenopus laevis* metamorphosis. *Proc Natl Acad Sci U S A* 102: 12455–12458; 2005. doi:10.1073/pnas.0505989102.

Cameron J. A.; Fallon J. F. The absence of cell death during development of free digits in amphibians. *Dev Biol* 55: 331–338; 1977.

Daniels K.; Reiter R.; Solursh M. Micromass cultures of limb and other mesenchyme. *Methods Cell Biol* 51: 237–247; 1996.

Das B.; Cai L.; Carter M. G.; Piao Y. L.; Sharov A. A.; Ko M. S.; Brown D. D. Gene expression changes at metamorphosis induced by thyroid hormone in *Xenopus laevis* tadpoles. *Dev Biol* 291: 342–355; 2006. doi:10.1016/j.ydbio.2005.12.032.

Denker A. E.; Nicoll S. B.; Tuan R. S. Formation of cartilage-like spheroids by micromass cultures of murine C3H10T1/2 cells upon treatment with transforming growth factor-beta 1. *Differentiation* 59: 25–34; 1995. doi:10.1046/j.1432-0436.1995.5910025.x.

Fallon J. F.; Cameron J. Interdigital cell death during limb development of the turtle and lizard with an interpretation of evolutionary significance. *J Embryol Exp Morphol* 40: 285–289; 1977.

Ganān Y.; Macias D.; Duterque-Coquillaud M.; Ros M. A.; Hurle J. M. Role of TGF beta s and BMPs as signals controlling the position of the digits and the areas of interdigital cell death in the developing chick limb autopod. *Development* 122: 2349–2357; 1996.

Gavrieli Y.; Sherman Y.; Ben-Sasson S. A. Identification of programmed cell death in situ via specific labeling of nuclear DNA fragmentation. *J Cell Biol* 119: 493–501; 1992.

Guha U.; Gomes W. A.; Kobayashi T.; Pestell R. G.; Kessler J. A. *In vivo* evidence that BMP signaling is necessary for apoptosis in the mouse limb. *Dev Biol* 249: 108–120; 2002.

Hamburger V.; Hamilton H. A series of normal stages in the development of the chick embryo. *J Morphol* 88: 49–92; 1951.

Hernandez-Martinez R.; Covarrubias L. Interdigital cell death function and regulation: new insights on an old programmed cell death model. *Dev Growth Differ* 53: 245–258; 2011. doi:10.1111/j.1440-169X.2010.01246.x;10.1111/j.1440-169X.2010.01246.x.

Hinchliffe J. R.; Thorogood P. V. Genetic inhibition of mesenchymal cell death and the development of form and skeletal pattern in the limbs of *talpid3* (*ta3*) mutant chick embryos. *J Embryol Exp Morphol* 31: 747–760; 1974.

Iwasawa H.; Kera Y. Normal stages of development of the Japanese lungless salamander, *Onychodactylus japonicus* (houttuyn). (in Japanese: Abstract in English). *Jpn J Herpetol* 8: 73–89; 1980.

Kaltenback J. C. Local action of thyoxin on amphibian metamorphosis. I. Local metamorphosis in *Rana pipiens* larvae effected by thyroxin-cholesterol implants. *J Exp Zool* 122: 21–23; 1953.

Kerr J. F.; Harmon B.; Searle J. An electron-microscope study of cell deletion in the anuran tadpole tail during spontaneous metamorphosis with special reference to apoptosis of striated muscle fibers. *J Cell Sci* 14: 571–585; 1974.

Kim M.; Kim S. E.; Kang S. S.; Kim Y. H.; Tae G. The use of de-differentiated chondrocytes delivered by a heparin-based hydrogel to regenerate cartilage in partial-thickness defects. *Biomaterials* 32: 7883–7896; 2011. doi:10.1016/j.biomaterials.2011.07.015;2011.

Lippens S.; Hoste E.; Vandenabeele P.; Agostinis P.; Declercq W. Cell death in the skin. *Apoptosis* 14: 549–569; 2009. doi:10.1007/s10495-009-0324-z.

Macias D.; Ganan Y.; Sampath T. K.; Piedra M. E.; Ros M. A.; Hurle J. M. Role of BMP-2 and OP-1 (BMP-7) in programmed cell death and skeletogenesis during chick limb development. *Development* 124: 1109–1117; 1997.

Montero J. A.; Hurle J. M. Sculpturing digit shape by cell death. *Apoptosis* 15: 365–375; 2010. doi:10.1007/s10495-009-0444-5.

Nieuwkoop P. D.; Faber J. Normal Table of *Xenopus laevis* (Daudin). North-Holland, Amsterdam; 1967.

Nishikawa A.; Kaiho M.; Yoshizato K. Cell death in the anuran tadpole tail: thyroid hormone induces keratinization and tail-specific growth inhibition of epidermal cells. *Dev Biol* 131: 337–344; 1989.

Nishikawa A.; Yoshizato K. Hormonal regulation of growth and life span of bullfrog tadpole tail epidermal cells cultured in vitro. *J Exp Zool* 237: 221–230; 1986. doi:10.1002/jez.1402370208.

Nye H. L.; Cameron J. A. Strategies to reduce variation in *Xenopus* regeneration studies. *Dev Dyn* 234: 151–158; 2005. doi:10.1002/dvdy.20508.

Omi M.; Sato-Maeda M.; Ide H. Role of chondrogenic tissue in programmed cell death and BMP expression in chick limb buds. *Int J Dev Biol* 44: 381–388; 2000.

Roberts L. M.; Hirokawa Y.; Nachtigal M. W.; Ingraham H. A. Paracrine-mediated apoptosis in reproductive tract development. *Dev Biol* 208: 110–122; 1999. doi:10.1006/dbio.1998.9190.

Roth K. A.; D'Sa C. Apoptosis and brain development. *Ment Retard Dev Disabil Res Rev* 7: 261–266; 2001. doi:10.1002/mrdd.1036.

Salas-Vidal E.; Valencia C.; Covarrubias L. Differential tissue growth and patterns of cell death in mouse limb autopod morphogenesis. *Dev Dyn* 220: 295–306; 2001. doi:10.1002/dvdy.1108.

Samuels H. H.; Stanley F.; Casanova J. Depletion of L-3,5,3'-triiodothyronine and L-thyroxine in euthyroid calf serum for use in cell culture studies of the action of thyroid hormone. *Endocrinology* 105: 80–85; 1979.

Satoh A.; Suzuki M.; Amano T.; Tamura K.; Ide H. Joint development in *Xenopus laevis* and induction of segmentations in regenerating froglet limb (spike). *Dev Dyn* 233: 1444–1453; 2005. doi:10.1002/dvdy.20484.

Saunders Jr. J. W.; Fallon J. F. Cell death in morphogenesis. In: Locke M. (ed) Major problems in developmental biology. Academic Press, New York, pp 289–314; 1966.

Saunders Jr. J. W.; Gasseling M. T. Cellular death in morphogenesis of the avian wing. *Dev Biol* 5: 147–178; 1962.

Shibota Y.; Kaneko Y.; Kuroda M.; Nishikawa A. Larval-to-adult conversion of a myogenic system in the frog, *Xenopus laevis*, by larval-type myoblast-specific control of cell division, cell differentiation, and programmed cell death by triiodo-L-thyronine. *Differentiation* 66: 227–238; 2000. doi:10.1046/j.1432-0436.2000.660409.x.

Sohn S. J.; Thompson J.; Winoto A. Apoptosis during negative selection of autoreactive thymocytes. *Curr Opin Immunol* 19: 510–515; 2007. doi:10.1016/j.coi.2007.06.001.

Tallheden T.; Karlsson C.; Brunner A.; Van Der Lee J.; Hagg R.; Tommasini R.; Lindahl A. Gene expression during redifferentiation of human articular chondrocytes. *Osteoarthr Cartil* 12: 525–535; 2004. doi:10.1016/j.joca.2004.03.004.

Tang M. K.; Leung A. K.; Kwong W. H.; Chow P. H.; Chan J. Y.; Ngo-Muller V.; Li M.; Lee K. K. Bmp-4 requires the presence of the digits to initiate programmed cell death in limb interdigital tissues. *Dev Biol* 218: 89–98; 2000. doi:10.1006/dbio.1999.9578.

Tesniere A.; Panaretakis T.; Kepp O.; Apetoh L.; Ghiringhelli F.; Zitvogel L.; Kroemer G. Molecular characteristics of immunogenic cancer cell death. *Cell Death Differ* 15: 3–12; 2008. doi:10.1038/sj.cdd.4402269.

Theiler K. The house mouse: atlas of embryonic development. Springer-Verlag, New York; 1989.

Togo S.; Sato T.; Sugiura H.; Wang X.; Basma H.; Nelson A.; Liu X.; Bargar T. W.; Sharp J. G.; Rennard S. I. Differentiation of embryonic stem cells into fibroblast-like cells in three-dimensional type I collagen gel cultures. *In Vitro Cell Dev Biol Anim* 47: 114–124; 2011. doi:10.1007/s11626-010-9367-2.

Tone S.; Tanaka S.; Kato Y. The inhibitory effect of 5-bromodeoxyuridine on the programmed cell death in the chick limb. *Dev Growth Differ* 25: 381–391; 1983.

Yokouchi Y.; Sakiyama J.; Kameda T.; Iba H.; Suzuki A.; Ueno N.; Kuroiwa A. BMP-2/-4 mediate programmed cell death in chicken limb buds. *Development* 122: 3725–3734; 1996.

Yokoyama H.; Endo T.; Tamura K.; Yajima H.; Ide H. Multiple digit formation in *Xenopus* limb bud recombinants. *Dev Biol* 196: 1–10; 1998. doi:10.1006/dbio.1998.8856.

Zou H.; Niswander L. Requirement for BMP signaling in interdigital apoptosis and scale formation. *Science* 272: 738–741; 1996.

Zuzarte-Luis V.; Hurle J. M. Programmed cell death in the embryonic vertebrate limb. *Semin Cell Dev Biol* 16: 261–269; 2005. doi:10.1016/j.semcdb.2004.12.004.